A New Longwave Mode Propagator for the Earth-Ionosphere Waveguide

Forrest Gasdia and Robert A. Marshall, Member, IEEE

Abstract—Very low frequency (VLF) radio waves propagate efficiently over long distances in the naturally occurring Earthionosphere waveguide. These radio waves are emitted by both natural and man-made sources and have been used for navigation and global communication systems and as a means to remotely sense the lower ionosphere. Propagation models are required to design and analyze longwave radio links and act as a forward model in the nonlinear inversion of receiver measurements to estimate the ionosphere. We have developed software that applies mode theory to calculate the distant fields produced by a dipole emitter in the Earth-ionosphere waveguide. This model, released as the Julia package LongwaveModePropagator.jl, is similar to the Long-Wavelength Propagation Capability (LWPC), but replaces the mode solver with the Global complex Roots and Poles Finding (GRPF) algorithm. As a result, mode finding is more robust and the model is simplified by solving the physical mode equation. This paper presents an overview of the model physics and validates the new Longwave Mode Propagator by comparing results with different ionospheres to LWPC and a finite-difference time-domain (FDTD) propagation model. As an example of its use, we briefly explore the relationship between exponential and Faraday-International Reference Ionosphere (FIRI) electron density profiles.

Index Terms—Very low frequency (VLF), Earth-ionosphere waveguide, Long-Wavelength Propagation Capability (LWPC), propagation model.

I. INTRODUCTION

The space between Earth's surface and the *D*-layer at the base of the ionosphere acts as a naturally occurring waveguide for the propagation of long radio waves at the low frequency (LF, 30–300 kHz) radio band and below. Whether generated naturally by lightning discharges or artificially by transmitters, longwaves efficiently propagate over global distances within the Earth-ionosphere waveguide (EIWG) [1]. This phenomenon has been exploited by long-range navigation and communication systems for decades [2]–[4]. Long radio waves propagating in the EIWG are also used to remotely sense the electromagnetic properties of the ground and *D*-layer of the ionosphere that affect the field pattern in the waveguide [5]–[7].

Longwave propagation models for the Earth-ionosphere waveguide are used to assess the expected performance and

Manuscript received January 30, 2021; revised April 06, 2021; accepted May 16, 2021. This project was supported by a fellowship award through the National Defense Science and Engineering Graduate (NDSEG) Fellowship Program, sponsored by the Air Force Research Laboratory (AFRL), the Office of Naval Research (ONR) and the Army Research Office (ARO), and the National Science Foundation VIPER project under grant AGS 1952465. (Corresponding author: Forrest Gasdia).

F. Gasdia and R. A. Marshall are with the Ann and H.J. Smead Department of Aerospace Engineering Sciences, University of Colorado Boulder, Boulder, CO, 80303 (e-mail: forrest.gasdia@colorado.edu).

robustness of very low frequency (VLF, 3–30 kHz) communication and navigation channels under a range of ionospheric conditions [8], [9]. Governments are the primary users of the VLF band and often require analysis of their links under rare or unnatural conditions, such as nuclear environments, which are not conducive to experimental study [10]. Examples of networks designed and evaluated with input from propagation models include the Minimum Essential Emergency Communication Network (MEECN) and the now-retired Omega navigation system [11], and recently there has been renewed interest in VLF positioning systems [12], [13].

Scientific studies of the lower ionosphere using subionospheric long radio waves also require computer propagation models for all but the simplest experiments. Both lightninggenerated radio atmospherics ("sferics") and man-made narrowband transmitter signals have been used as radio sources to probe the ionosphere [14], [15]. The quantity of interest is the electron density profile from ground up into the ionosphere averaged along the propagation path from emitter to receiver, and the observed quantity, after processing, is typically the vertical electric field amplitude and phase of the transmitted signal. Magnetic field components and signal polarization can also be observed [16]. The relationship between the observation at a receiver and the ionosphere electron density profile is complicated and additionally depends on Earth curvature, the background magnetic field, electrical properties of the ground, and the collision frequency profile along the propagation path, plus higher order effects [17]–[20]. Inversion of the observations to obtain an estimate of the electron density profile is underdetermined. Its solution requires a nonlinear or iterative method that uses a propagation model as the forward model [21], [22].

Several propagation models have been developed for long-wave propagation in the EIWG. They can broadly be categorized as: finite element or finite difference models, ray theory models, or mode theory models. In all cases, an accurate solution of Maxwell's equations is required because the incident electromagnetic wave is partially reflected, partially penetrating, and partially absorbed [23]. Unlike ionospheric propagation models of high frequency (HF, 3–30 MHz) radio waves where a geometric optics approach is applicable, "full wave" solutions are required at low frequencies where the electromagnetic characteristics of the ionosphere change considerably within the distance of a VLF free-space wavelength (10–100 km); this violates the geometric optics assumption of a slowly varying medium [24].

Finite element methods solve a discretized form of

Maxwell's equations on a spatial grid. Several finite element models have been constructed for longwave propagation, including: two- and three-dimensional finite-difference time-domain (FDTD) [25], [26], finite-difference frequency-domain (FDFD) [26], and a recursive approach known as the Stanford Full-wave Method (FWM) [27], [28]. Finite element models provide electric field and other quantities at a high resolution across the model grid and can incorporate complex structures in the EIWG. Although capable models, finite element approaches require greater computational resources than the other methods. FDFD requires large matrix inversions and FDTD has a numerical stability requirement to resolve the wave propagation in space and time [29]. The FWM has a step size requirement that scales its number of integrations with the distance of interest from the emitter squared [28].

Ray theory models are less common than the other approaches, but can be efficient at short ranges from the emitter. The total field is expressed as the sum of a number of ray "hops" off the ionosphere and ground. Relatively few hops are required at short ranges on the order of 100 km, but at greater distances a large number of hops must be considered [30]. A recently-developed ray model has been successfully employed to model lightning sferic propagation over ranges of hundreds up to a couple of thousand kilometers [31], [32].

The best-known longwave propagation computer code is possibly the Long-Wavelength Propagation Capability (LWPC), which is based on mode theory and has been used both as an operational aid for signal coverage analysis [33], [34] and as a scientific tool, e.g. [35]. LWPC is a collection of several integrated programs developed between the 1960s and 1990s by the U.S. Naval Electronics Laboratory Center (NELC), which later merged into the Naval Ocean Systems Center (NOSC), and then Space and Naval Warfare Systems Command (SPAWAR) during development of the model [36]-[40]. The complicated propagation model within LWPC treats the EIWG as free space bounded by a reflecting wall at the ground and a reflecting wall at the ionosphere. Resonant eigenangles of the waveguide are identified and the electric field corresponding to each is calculated at a receiver position in the waveguide and summed over all modes. Details of the theory will be discussed in Section II. The model is heavily analytical and significant effort was made to maximize the compute efficiency and minimize runtime. In the decades over which LWPC was developed to now, computer processing power has increased by several orders of magnitude [41]. Today, calculating the electric field in the waveguide over thousands of kilometers takes just seconds on a personal computer.

Despite the great utility offered by its speed, and its long heritage as a VLF propagation model, LWPC has several shortcomings. The mode finder, described in [38] with some alterations presented in [42], makes extensive use of interpolation that was identified during its development as the weakest link in locating eigenangles. It also requires significant transformation of the physical equations to remove poles from the region of the complex plane on which the eigenangles lie. Numerical difficulties occur in the LF band [43] and we have also observed numerical problems or program failure for

ionospheres which do not have a sharp electron density profile (low β using Wait's exponential ionosphere parameters [44]). There are practical downsides to LWPC as well. As previously mentioned, the LWPC propagation model is a collection of separately developed programs that work together, yet each remain relatively self-contained within LWPC. Many of these "submodules" then provide redundant functionality with other submodules, albeit with slightly different implementations or even different hard-coded values for parameters such as Earth radius. Copies of LWPC in use by different researchers have begun to diverge as "fixes" for the multiple hard-coded definitions of Earth radius, mode finder search region, or minimum and maximum ionospheric heights are altered [35]. Various memory errors have also been reported [45].

This paper introduces a new mode theory model which we refer to as the Longwave Mode Propagator (LMP). LMP replaces LWPC's mode finder with the Global complex Roots and Poles Finding (GRPF) algorithm [46] which allows for a simplification of many of LWPC's solution steps. The code is freely available and written in the Julia programming language, which allows it to be run on all major modern operating systems. In Section II, an overview of each step of the propagation model is presented. Section III discusses the Longwave Mode Propagator software package and contrasts it with LWPC. Section IV validates LMP against LWPC and an FDTD model. This serves both as a check on accuracy of the new model and as an example of its use. Finally, a summary and suggestions for improvement are presented in Section V.

II. WAVEGUIDE MODE PROPAGATION MODEL

Although the treatment of longwave propagation problems had used a concentric conducting shell around Earth for several decades and wave interference had been experimentally observed [47], [48], the waveguide mode theory employed by both LWPC and the new Longwave Mode Propagator was largely developed by K. G. Budden in the 1950s. In [49], an approach is presented to calculate the reflection coefficient of the anisotropic ionosphere as though it were a sharp boundary, and in [50] Budden presented the mode theory to calculate the fields from a known exciter in the waveguide. By year 1967, results from a computer program developed at the U.S. Navy Electronics Laboratory using Budden's formalism were published [17]. A number of others worked on implementation details and will be cited below.

A good overview of the theory of long radio wave propagation in the EIWG is presented in [50]. The theory allows for general electron density and collision frequency profiles of the ionosphere, profiles for additional species, Earth's magnetic field, and it accounts for Earth's curvature. The system is modeled with Earth's surface and the ionosphere forming two walls of a waveguide with free space in the middle. If a radio source is placed in the space of the waveguide, the amplitude of the wave excited in a given mode can be calculated at some other point in the guide. The total field observed at that point is the sum of the fields corresponding to each propagating mode. Therefore, the two major tasks of a mode theory propagation program are to identify the resonant modes



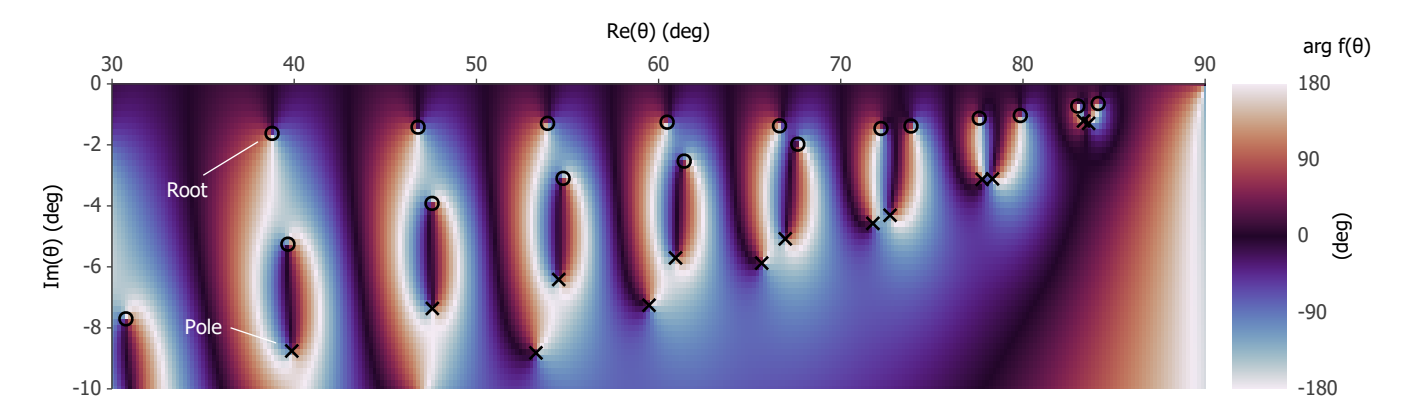


Fig. 1. Complex phase of the mode equation, eq. (4), for a 20 kHz wave and a typical daytime ionosphere with h' = 75, $\beta = 0.35$, and associated collision frequency profile [51]. Roots of the equation are marked with \circ and poles are marked with \times . The background magnetic field is vertical with a strength of $50\,000\,\mathrm{nT}$ and the ground conductivity is $0.001\,\mathrm{S}\,\mathrm{m}^{-1}$.

and to calculate the wave fields of each mode. Over long propagation paths, it is inevitable that the electrical properties of either the ionosphere or ground, or both, will change. The resonant modes of each homogeneous segment of the EIWG can be determined independently. Then, the field produced by a radio source in a different segment of the waveguide can be propagated into the next segment by mode conversion [52].

This section briefly explains the key components of EIWG modal propagation models. The coordinate system used has x along the planar waveguide, z directed upward into the ionosphere, and y completes the right-handed coordinate system perpendicular to the waveguide. Propagation occurs in the x-z plane and invariance is assumed in y.

A. Mode Finding

The mode finder task is to identify resonant waveguide modes. This process is usually limited to finding a subset of discrete modes that have the greatest influence on the total observed field. Each mode can be thought to correspond with a plane wave propagating at an angle θ from the vertical. This is often referred to as an eigenangle because they are discrete eigenvalues of a differential equation [50]. It follows that the wave propagation is described by the factor $\exp(-ik(x\sin\theta + z\cos\theta))$ for wavenumber k. It can also be assumed to vary in time t by a factor $\exp(i\omega t)$ for angular frequency ω , but for simplicity this term will not be written. The eigenangle θ is generally complex-valued and the phase velocity and attenuation of the mode are proportional to $c/\operatorname{Re}(\sin\theta)$ and $\operatorname{Im}(\sin\theta)$, respectively, for propagation velocity c. It follows that the most influential modes are those with eigenangles having small imaginary components (with low attenuation) and large real components (with high group velocity).

1) Fundamental Equation of Mode Theory: Consider the waveguide bounded by reflecting boundaries at heights z=0 and z=h with reflection coefficients $R_0(\theta)$ and $R_h(\theta)$, respectively. Each reflection coefficient is simply the ratio of the downgoing to the upgoing field, referenced to a particular height.

Budden, in [53, ch. 8], writes expressions for a field component of three waves. The first is an upgoing plane

wave with amplitude F_1 , the second is an ionosphere-reflected downgoing plane wave F_2 , and finally an ionosphere- and ground-reflected upgoing plane wave F_3 . The condition for the two crossing waves F_1 and F_2 to propagate as a mode down the waveguide is that F_3 must be identical to F_1 . From the expressions for the fields, it is simple to derive the requirement

$$R_0(\theta)R_h(\theta)\exp(-2ikh\cos\theta) = 1 \tag{1}$$

which is known as the fundamental equation of mode theory. Each discrete θ for which this criteria is met represents a waveguide mode. Eq. (1) is true for any boundaries of reflection with known reflection coefficients, even for a stratified medium like the ionosphere. In order to satisfy eq. (1) when the boundaries are not perfect reflectors, θ must include an imaginary component.

The ionosphere's anisotropy also requires that the twice reflected wave have identical polarization with the original upgoing wave. Therefore, the reflection coefficients are treated as matrices

$$\mathbf{R}(\theta) = \begin{pmatrix} {}_{\parallel}R_{\parallel} & {}_{\perp}R_{\parallel} \\ {}_{\parallel}R_{\perp} & {}_{\perp}R_{\perp} \end{pmatrix} \tag{2}$$

where the pre-subscript indicates the component polarization of the incident wave and the post-subscript indicates the polarization of the reflected wave. Subscript " $\|$ " indicates the electric field is parallel to the x-z plane of incidence and " \bot " indicates the electric field is perpendicular, in y. If the column vector e contains the electric field components parallel and perpendicular to the plane of incidence, then the mode equation can be expressed as

$$\mathbf{R}_0(\theta)\mathbf{R}_h(\theta)\mathbf{e} = \mathbf{I}\mathbf{e} \tag{3}$$

where I is the 2×2 identity matrix and both reflection coefficient matrices are referenced to the ground at height z=0 such that the exponential in eq. (1) equals unity. This eigenvalue problem requires the square matrix $R_0R_h - I$ be singular for a nontrivial eigenvector e to exist. This is true if

$$\det(\mathbf{R}_0(\theta)\mathbf{R}_h(\theta) - \mathbf{I}) = 0. \tag{4}$$

The left hand side of eq. (4) is a complex-valued function with complex arguments. The purpose of the mode finder is to identify eigenangles θ at which roots of this function occur.

Fig. 1 depicts the complex phase of the left side of eq. (4) throughout a portion of the bottom right quadrant of the complex plane on which physical solutions of eq. (4) lie. The lowest order modes occur at roots towards the top right of the figure; these modes have the smallest imaginary part of θ and thus the lowest attenuation, and a large $\mathrm{Re}(\theta)$ implies a propagation direction largely along the waveguide. The reflection coefficients and wave frequency have a tremendous effect on the position and density of the roots and poles on the complex plane.

2) Ionosphere Reflection Coefficient: The reflection coefficient matrix for the ionosphere, corresponding to \mathbf{R}_h in the section above, is derived from Maxwell's equations for an electromagnetic wave in the collisional, anisotropic cold plasma of the ionosphere. Several derivations of these equations can be found [54]–[56]. Clemmow and Heading wrote them in matrix form

$$\frac{\mathrm{d}\boldsymbol{e}}{\mathrm{d}z} = -ik\boldsymbol{T}\boldsymbol{e} \tag{5}$$

with respect to height z where e is the column vector $(E_x, -E_y, \mathcal{H}_x, \mathcal{H}_y)^{\top}$ for electric field components E and magnetic field components $\mathcal{H} = Z_0H$ where Z_0 is vacuum impedance. The 4×4 matrix T contains elements of the magnetic susceptibility tensor expressed for an obliquely incident plane wave in our coordinate frame. Derivations of the susceptibility tensor from the constitutive relations can be found elsewhere [56], [57], but it is important to note that the susceptibility tensor is a function of the electron density and collision frequency, and is therefore a function of height.

Earth curvature is accounted for in LWPC and LMP by including a fictitious refractive index term in the susceptibility matrix, which is based on a technique first suggested by Booker and Walkinshaw [58]. The first order correction is simply to subtract $(2/R_e)(H-z)$ from the diagonal elements of the susceptibility matrix where R_e is Earth radius and H is a reference height where the refractive index $\mathfrak{n}=1$. This method of including Earth curvature has been found to generally agree with analytical calculations of VLF propagation performed in a spherical coordinate frame and with a rigorous conformal transformation [17], [59].

Budden presents two solutions for the ionosphere reflection coefficient matrix in [49]. Both LWPC and the Longwave Mode Propagator use his second method of solution, which derives the differential of \boldsymbol{R} with respect to height z from T transformed for components of an upgoing and downgoing wave. The differential equation for \boldsymbol{R} is

$$\frac{2i}{k}\frac{\mathrm{d}\boldsymbol{R}}{\mathrm{d}z} = \boldsymbol{W}_{21} + \boldsymbol{W}_{22}\boldsymbol{R} - \boldsymbol{R}\boldsymbol{W}_{11} - \boldsymbol{R}\boldsymbol{W}_{12}\boldsymbol{R}$$
(6)

where W is the transformed version of T partitioned into four submatrices.

Assuming R is known at some initial height high in the ionosphere, then eq. (6) can be integrated downwards through the ionosphere. At whatever height the integration is stopped, the result is the reflection coefficient corresponding to a sharp boundary at that level with free space below. The right side of Fig. 2 shows the four components of R as they are integrated through the ionosphere described by the exponential profiles

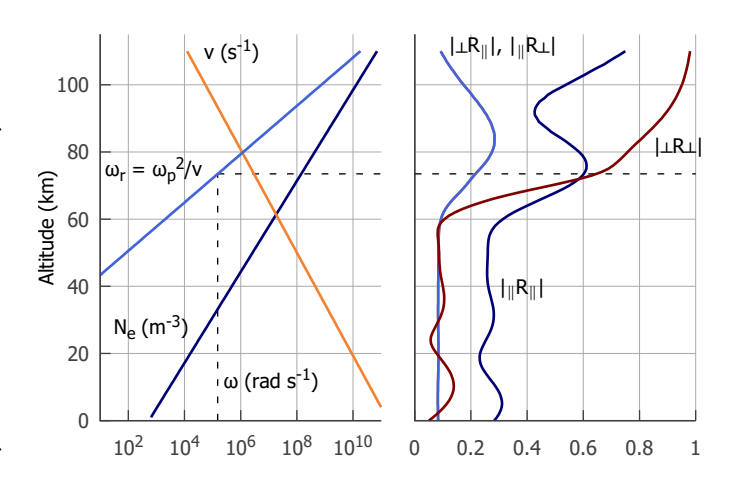


Fig. 2. Left: Profiles of electron density N_e , collision frequency ν , and Wait's conductivity parameter ω_r for an ionosphere with h'=75 and $\beta=0.32$ and a vertical magnetic field of 50 000 nT. Right: Components of the ionosphere reflection coefficient (unitless) integrated downwards for a 24 kHz radio wave at an angle of incidence of 75° from the ionosphere. The bulk of the reflection occurs approximately at the height where ω_r equals the angular wave frequency ω .

shown on the left. The bulk of the wave reflection occurs approximately at the height where the ratio of the plasma frequency squared ω_p^2 over the collision frequency ν , a quantity known as Wait's parameter ω_r [44], is equal to the angular wave frequency [57]. As the integration proceeds through the bottom of the ionosphere into what is nearly free space, the diagonal elements of the matrix R begin to follow a sinusoidal pattern. The off-diagonal elements in Fig. 2 are equal because a vertical magnetic field is used.

The starting solution for the ionosphere reflection coefficient matrix at a great height is obtained using a solution for a sharply bounded homogeneous ionosphere. There are several approaches to calculating such a reflection coefficient. Budden conducts a preliminary integration through a vertically homogeneous ionosphere until $\mathrm{d}\mathbf{R}/\mathrm{d}z$ reaches a sufficiently small value [49]. Sheddy presents a closed solution which is used in LWPC [60]. The solution makes use of the Booker quartic [61], [62] and is simplified by the use of Budden's coordinate system. Of the four quartic roots q_i , two correspond to characteristic obliquely upgoing waves and two to downgoing waves. At a great height in the ionosphere, there should only exist upgoing waves.

Budden, in [56, ch. 7], inspires a similar approach using wavefields for the characteristic upgoing waves that is implemented in the Longwave Mode Propagator. For a homogeneous ionosphere, T is independent of z and the wavefields depend on z only through the factor $\exp(-ikqz)$. Eq. (5) then results in the eigenvalue problem Te=qe. The roots of the Booker quartic q are found iteratively using the software library PolynomialRoots.jl [63]. We choose $e_2=1$, immediately leading to $e_3=q$. The remaining two unknowns are solved from the three remaining equations. Scaling of these fields can be arbitrary for calculating the reflection coefficient matrix so long as their ratios are maintained. The two wavefield vectors e_1 and e_2 , corresponding to the two upgoing waves, are resolved into up- and down-going vacuum

plane components. If the vectors of complex amplitudes for these components are called f and g, then the reflection coefficient matrix is

$$\mathbf{R} = \mathbf{D}\mathbf{U}^{-1} = \begin{pmatrix} f_3 & g_3 \\ f_4 & g_4 \end{pmatrix} \begin{pmatrix} f_1 & g_1 \\ f_2 & g_2 \end{pmatrix}^{-1}.$$
 (7)

Although not shown in detail, this approach is similar to that used to derive eq. (6).

3) Ground Reflection Coefficient: Evaluating the mode equation, eq. (4), also requires the reflection coefficient matrix of the ground R_0 . LWPC and the Longwave Mode Propagator both make the assumption that the ground is isotropic and vertically homogeneous. Therefore, the reflection coefficient matrix is described by the well-known Fresnel reflection equations for transverse magnetic and transverse electric fields [64]. The ground reflection coefficient matrix is given by

$$\boldsymbol{R}_0 = \begin{pmatrix} {}_{\parallel}\boldsymbol{R}_{\parallel 0} & \boldsymbol{0} \\ \boldsymbol{0} & {}_{\perp}\boldsymbol{R}_{\perp 0} \end{pmatrix} \tag{8}$$

where

$${}_{\parallel}R_{\parallel0} = \frac{\mathfrak{n}_0^2 \cos\theta - \left(\mathfrak{n}_0^2 - \sin^2\theta\right)^{1/2}}{\mathfrak{n}_0^2 \cos\theta + \left(\mathfrak{n}_0^2 - \sin^2\theta\right)^{1/2}} \tag{9}$$

$${}_{\perp}R_{\perp 0} = \frac{\cos\theta - \left(\mathfrak{n}_0^2 - \sin^2\theta\right)^{1/2}}{\cos\theta + \left(\mathfrak{n}_0^2 - \sin^2\theta\right)^{1/2}} \tag{10}$$

and the squared index of refraction $\mathfrak{n}_0^2=\epsilon_r-i\sigma/\omega\epsilon_0$ assuming relative permeability $\mu_r\approx 1$.

B. Waveguide Field Sum

Given our model of the EIWG with a ground reflecting boundary, ionosphere reflecting boundary, and free space in between, the E_y field in the z axis of the waveguide satisfies the wave equation

$$\frac{\mathrm{d}^2 E_y}{\mathrm{d}z^2} + k^2 q^2 E_y = 0. \tag{11}$$

By definition, $q^2 = n^2 - \sin^2 \theta$ [24], which becomes

$$q^2 = \cos^2 \theta - (2/R_e)(H - z) \tag{12}$$

when using a modified free-space index of refraction to simulate curved Earth. Morfitt and Shellman make the substitution [38]

$$\zeta = \left(\frac{k}{2/R_e}\right)^{2/3} q^2 \tag{13}$$

so that eq. (11) becomes

$$\frac{\mathrm{d}^2 E_y}{\mathrm{d}\zeta^2} + \zeta E_y = 0 \tag{14}$$

which is known as Stokes' equation and has the general solution

$$E_{\nu}(\zeta) = a_1 h_1(\zeta) + a_2 h_2(\zeta) \tag{15}$$

where h_1 and h_2 are the modified Hankel functions of order one third [65]. The constants a_1 and a_2 must be chosen so they are consistent with the waveguide boundaries.

Eq. (15) is known as the *height gain* function for the E_{ν} field component. Similar functions exist for E_x and E_z . Pappert and Shockey [66] present the height gain functions along with the appropriate constants to scale for the ground index of refraction and Earth curvature. Paired with the height gain functions are excitation factors which describe how efficiently a given field component is propagated in the waveguide. The excitation factor for each field component is determined by the elements of the reflection coefficient matrix that correspond to the appropriate wave polarization. This means that the fields emitted from a dipole source in the waveguide excite the guide differently depending on the orientation of the dipole, i.e. vertical, horizontal, or inclined with respect to the waveguide boundaries [50]. [66] also presents excitation factors and constructs them such that the total field produced in the waveguide by an arbitrarily oriented transmitting antenna is represented by a combination of vertical, end-on, and broadside-oriented dipole fields. The Longwave Mode Propagator uses an equivalent formulation, similar to the formulation in [67], that more explicitly separates the transmitter and receiver terms.

Once the mode finder has identified eigenangles of the waveguide, the total j=x,y,z component of the electric field produced by a dipole antenna measured by a receiver at height z_r and distance x from the transmitter is summed over each mode n as

$$E_j(x) = \frac{Q}{\left(\sin(x/R_e)\right)^{1/2}} \sum_n \Gamma_n \xi_n \exp\left(-ik(\sin(\theta_n) - 1)x\right)$$
(16)

where $\xi_n = f_{j,n}(z_r)$ is the receive antenna term and Γ_n is the transmitting antenna term

$$\Gamma_n = \lambda_{v,n} \cos(\gamma) f_{z,n}(z_t) + \lambda_{b,n} \sin(\gamma) \sin(\phi) f_{y,n}(z_t) + \lambda_{e,n} \sin(\gamma) \cos(\phi) f_{x,n}(z_t)$$
(17)

at height z_t , angle γ from the vertical and angle ϕ from the x direction [68]. The height gain functions for each field component j are notated with $f_{j,n}$ and excitation factors for each dipole orientation o = v, b, e for vertical, broadside, and end-on are notated with $\lambda_{o,n}$. Q is a scalar multiplier for the radiated power and frequency.

C. Mode Conversion

Upon transition from one segment of EIWG to a segment with different ground or ionosphere reflection coefficient, the energy in each mode is scattered into the modes that are supported by the next segment. Two primary approaches have been developed to model mode conversion for sharp transitions between waveguide segments: FASTMC [39] and FULLMC [69]. A mode can be described in terms of its height gain functions for each field component. At the transition between segments, continuity is required between the incident, reflected, and transmitted modes. Although it is generally possible that there are backward-propagating modes reflected at a second transition further down the waveguide, both methods simply ignore these reflections entirely. The ratio of transmitted to incident modes are used to calculate normalized

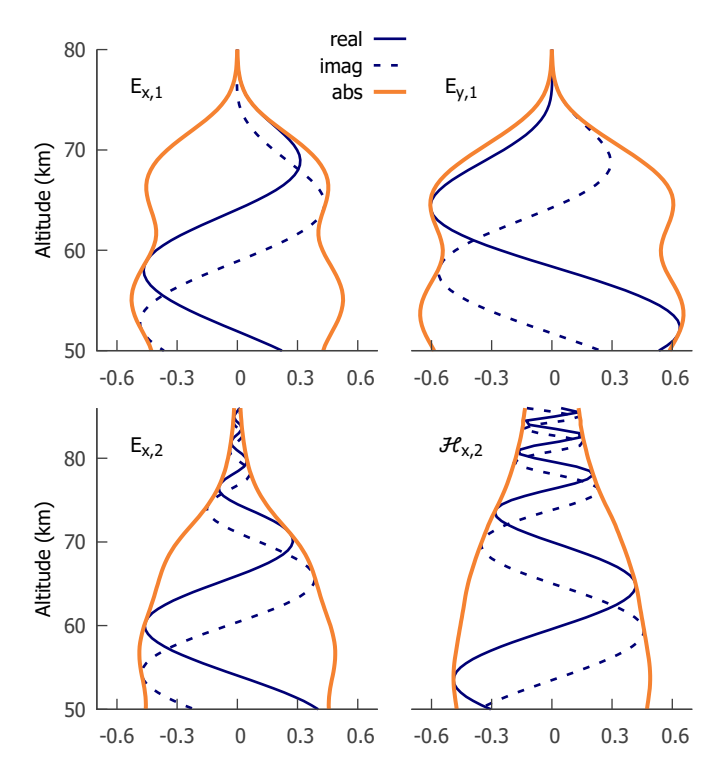


Fig. 3. Instantaneous wavefields set up by an incident wave of unit amplitude at the ground integrated through the ionosphere using the scaling method described by Pitteway in [70]. This figure is a reproduction of the same scenario used in [70, Fig. 2]. The upper curves are from the non-penetrating wave and the lower curves are from the penetrating wave.

conversion coefficients which can then be applied to the actual fields at each transition in the waveguide. Whereas FASTMC uses the modified Hankel functions to describe the height gain functions in each waveguide segment, FULLMC numerically integrates the wavefields between the ground and ionosphere. The Longwave Mode Propagator implements FULLMC using the integration method presented by [70].

The wavefield integration in LMP begins similarly to the starting condition for the reflection coefficient integration by calculating wavefields for a sharply bounded ionosphere from the Booker quartic. Then eq. (5) is numerically integrated downward through the ionosphere to the ground. Pitteway breaks the differential wave equations into solutions for penetrating and non-penetrating waves. The amplitudes of the two solutions varies greatly, causing numerical issues for double precision computers. Pitteway negates this by orthonormalizing the solutions during their integration to maintain their independence [70]. In the Longwave Mode Propagator, this is accomplished using callback functions in the DifferentialEquations.jl library [71]. Fig. 3 shows the amplitudes of four wavefield components in the D-layer integrated by this technique. For mode conversion all six components are integrated to the ground.

Eq. (16) in the previous section is for a homogeneous waveguide. A modified version which includes the mode conversion coefficients is required to calculate the fields in the waveguide segments after the segment with the transmitter. [68, eq. 23] provides the appropriate mode sum.

III. LONGWAVEMODEPROPAGATOR.JL

The Longwave Mode Propagator model is coded in the Julia programming language and is freely available under an MIT software license as the package LongwaveModePropagator.jl¹. The model currently supports the calculation of x, y, and zcomponents of the electric field in the EIWG produced by an arbitrarily oriented ground-based transmitter at a receiver located anywhere in the waveguide. It has been verified to produce reasonable results for transmitter frequencies from about 5 kHz to at least 100 kHz. The model runs on major modern operating systems (Windows, Linux, and macOS) and uses 64-bit precision floating point calculations throughout. It contains just over 2000 lines of source code, in comparison to LWPC's more than 26000 lines of Fortran, and is thoroughly documented. The package contains an automated test suite to compare many of the internal functions against alternate solutions.

The greatest flexibility is available by importing the package from within a Julia program. A parameters structure provides the user with the ability to define the integration methods, tolerance, Earth radius, and other parameters used throughout the model. By exposing many of these internal parameters, the user has much greater control than with LWPC. By default, reasonable values are used. The package can also read and write JSON formatted files for basic Wait or tabular ionosphere profiles if a user would rather interface with the model primarily from a scripting language such as Matlab or Python. The online package documentation includes examples of running the model from Julia and the JSON file interface.

Compared to LWPC, the Longwave Mode Propagator is a simpler model. Redundant functions are largely removed, the language's built-in linear algebra capabilities are exploited, and external packages provide functionality such as integration routines without building them into the model, as is done in LWPC. Perhaps most importantly, the model mathematics are greatly simplified by the introduction of an entirely new mode finder using the Global complex Roots and Poles Finding (GRPF) algorithm [46]. Unlike the mode finder used in LWPC, this algorithm identifies both roots and poles. A significant portion of the math used in LWPC is altered to accommodate a mode finder which does not properly function if there are poles in the domain. Therefore, in LWPC the ground and ionosphere reflection coefficients are modified, the mode equation is modified, and the reference height for reflection is dynamically calculated to reduce the probability of poles in the region of the complex plane being searched for roots. The Longwave Mode Propagator is able to solve the physical equations without modification and always integrates the ionosphere reflection coefficient to the ground. To new code contributors, this helps reduce confusion by removing the need to reference reflection heights and eigenangle heights up and down in the waveguide in different parts of the model.

The GRPF algorithm works by sampling the function being analyzed, eq. (4), at the nodes of a regular triangular mesh grid. The function's complex phase is analyzed and a discretized version of Cauchy's argument principle is applied to detect

¹https://github.com/fgasdia/LongwaveModePropagator.jl

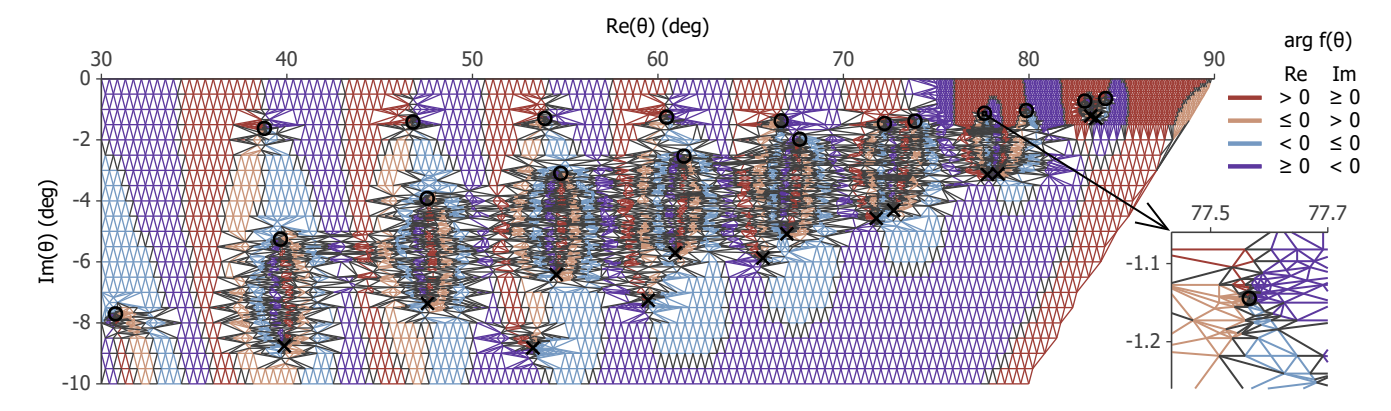


Fig. 4. The GRPF algorithm using the default initial mesh of LongwaveModePropagator.jl is applied to the same scenario as Fig. 1. As shown in the inset, the algorithm automatically refines the mesh to obtain more accurate estimates of the locations of roots and poles. Roots and poles, marked with o and x, respectively, are located at the points where the four quadrants of the function's complex phase meet. They are differentiated by using a discretized form of Cauchy's argument principle.

the presence of roots and/or poles inside candidate regions of the mesh. The mesh is automatically refined through Delaunay triangulation to obtain more accurate estimates of the positions of roots and poles. Compare Fig. 4, which applies the GRPF algorithm, to Fig. 1 [72]. The adaptive mesh refinement of GRPF locates roots and poles to better than 0.0005°. The method can also ensure that the entirety of a region of the complex plane is searched and that arbitrary regions can be excluded to save computation time. The default mesh used by LongwaveModePropagator.jl excludes the lower right diagonal of the lower right quadrant of the complex plane and uses a finer initial mesh in the top right corner where roots and poles may be very closely spaced.

The primary disadvantage of GRPF compared to the mode finder used by LWPC is computation time. The ionosphere reflection coefficient must be integrated at every node of the GRPF mesh, whereas LWPC actually interpolates the reflection coefficient and only integrates when the interpolation error estimate exceeds some threshold. Additionally, although GRPF cannot lose a root or pole once it has been detected, the initial mesh resolution must be fine enough such that there are an unequal number of roots and poles within each mesh triangle. Due to the way the discretized argument principle works, the method cannot determine if a mesh edge contour encircles no roots or poles or an equal number of roots and poles. If there is a single root or pole or an unequal number of roots and poles within the region being analyzed, then the mesh grid will be automatically refined to separate them. Even though the evaluation of the modal equation across the complex plane is multithreaded, LongwaveModePropagator.jl is roughly ten times slower than LWPC, with nearly all of the runtime spent on GRPF. With eight threads running on a six core i7-8700T CPU, LongwaveModePropagator.jl took 410 s to run 80 different homogeneous ionosphere scenarios whereas the single-threaded LWPC only took about 35 s. For the user, there is a trade-off between shorter runtime with LWPC and mode finding with the more robust GRPF algorithm of LMP. For the developer, use of GRPF simplifies the Longwave Mode Propagator code overall. In Section V, we discuss possible improvements to the LMP code that could reduce the run time

to be comparable to that of LWPC.

IV. MODEL VALIDATION

This section presents several validations of the Longwave Mode Propagator (LMP) against LWPC and the EMP2D two-dimensional FDTD model described in [26]. These are not meant to be exhaustive tests of the accuracy of LMP, rather they compare the results that may be obtained in practice across the three models. In some cases it is not clear which, if any, of the models produce the "correct" results. The final subsection, Section IV-D, demonstrates the use of tabular electron density and collision frequency profiles in a brief comparison of the Wait and FIRI ionosphere models [44], [73].

A. Wait Ionosphere Profiles

The amplitude of the vertical electric field along the ground is computed in 5 km increments from a 24 kHz transmitter out to 3000 km in a homogeneous ionosphere waveguide over an ocean-like surface. The magnetic field is 50 000 nT and is vertically oriented. Eighty different scenarios were run with unique ionospheres. The electron density profile is expressed using the h' and β parameters attributed to Wait [44]. The profile function is eq. (18), where the altitude z is in km and the electron density is in m⁻³. As is tradition, h' and β are implicitly in the units of km and km⁻¹, respectively.

$$N_e(z) = 1.43 \times 10^{13} \exp(-0.15h') \exp((\beta - 0.15)(z - h')).$$
(18)

The electron collision frequency profile associated with Wait's density profile is

$$\nu(z) = 1.816 \times 10^{11} \exp(-0.15z) \tag{19}$$

where ν is in s⁻¹ [51]. Unlike the density profile, the collision frequency profile is not parameterized.

For each of the comparison scenarios, LMP was run with default parameters using the package's BasicInput JSON file interface, which means that the ionosphere begins at 40 km altitude with free space below. LWPC was run using the homogeneous-exponential ionosphere specification. The Wait density and collision frequency profiles

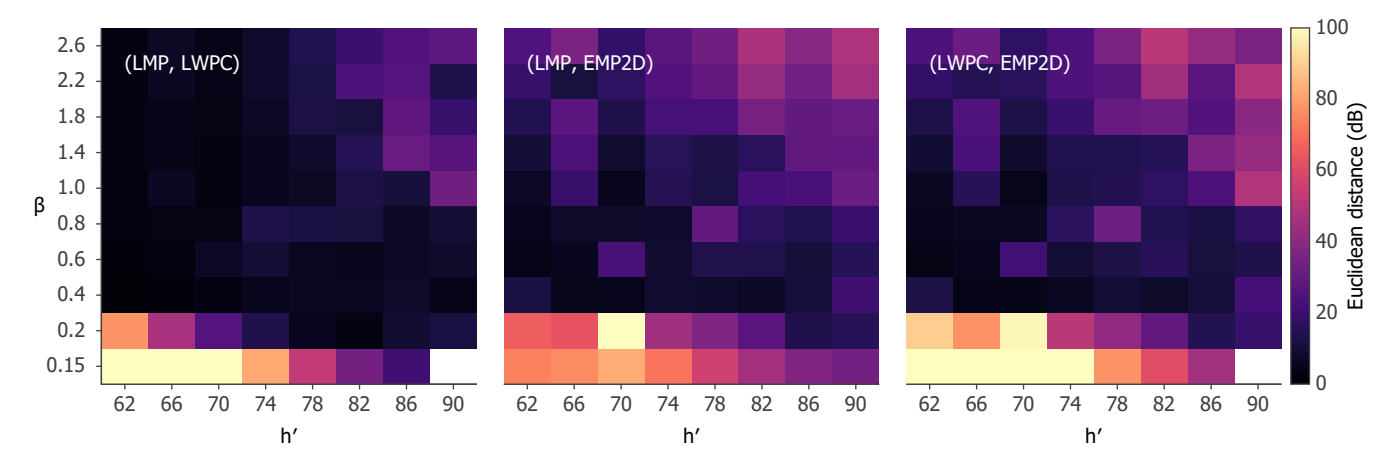


Fig. 5. Euclidean distance between the amplitude curves over 400 to 3000 km from the transmitter for each combination of the pairs of models LMP, LWPC, and EMP2D. Each scenario used a 24 kHz transmitter and had a vertical magnetic field and ocean-like ground conductivity. Note that the β values are not evenly distributed. The LWPC model failed for one of the scenarios with $\beta=0.15$.

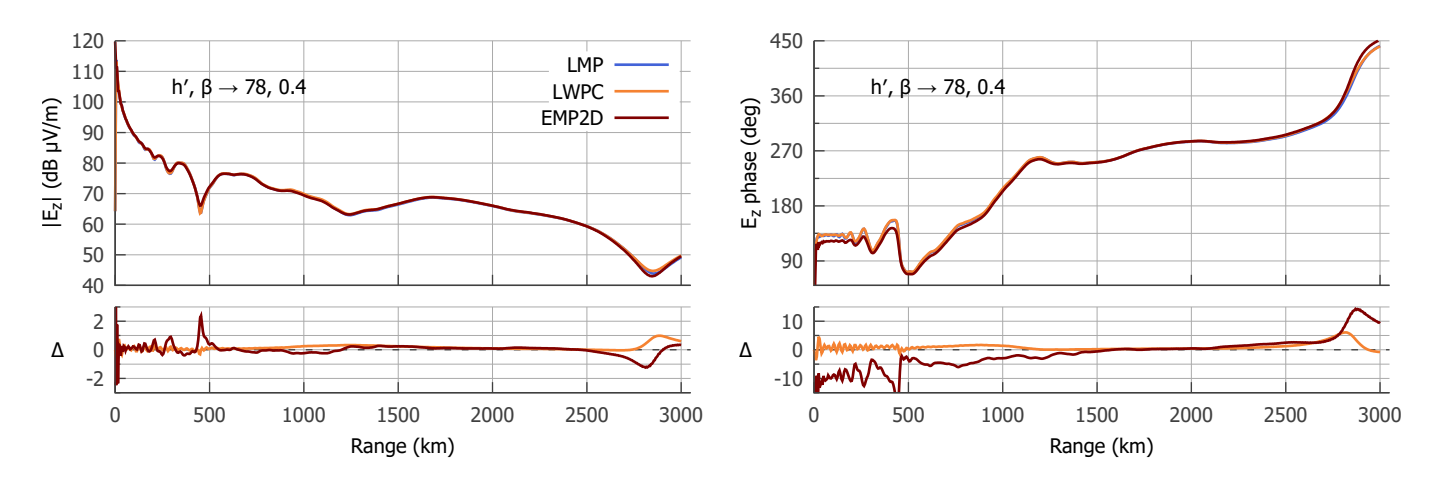


Fig. 6. Left: Vertical electric field amplitude for an ionosphere with an exponential profile specified by h'=78 and $\beta=0.4$. Right: Electric field phase for the same ionosphere. Both plots also show the difference Δ from LWPC and EMP2D to LMP.

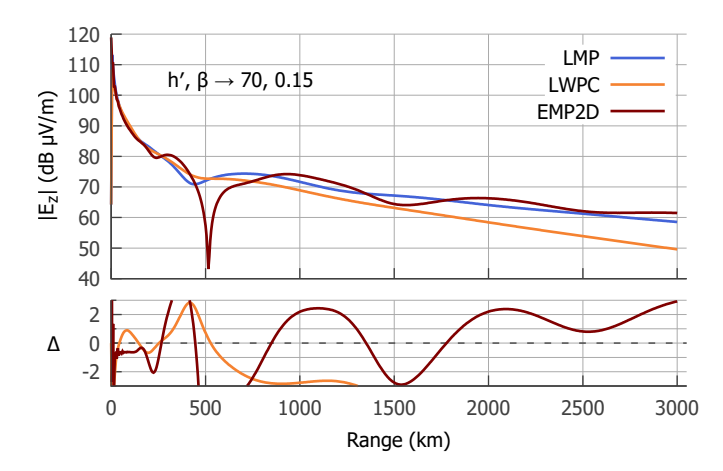


Fig. 7. Amplitude curves for an ionosphere with h'=70 and $\beta=0.15$. The EMP2D curve is shifted to minimize its Euclidean distance from the LMP curve alone, but the slope of the LMP curve is a better match to EMP2D than LWPC is

were tabulated on a $250\,\mathrm{m}$ vertical grid for EMP2D and the ionosphere began at $50\,\mathrm{km}$ altitude.

The Euclidean distance between the amplitude curves for

each model was computed over the range 400 to 3000 km from the transmitter and is summarized graphically in Fig. 5. Although LMP and LWPC are calibrated to transmitters with specified power levels, the EMP2D curve is shifted to minimize the Euclidean distance to LMP in the heatmap plot comparing LMP to EMP2D and is shifted to minimize the Euclidean distance to LWPC in the heatmap comparing LWPC to EMP2D. This is done to fairly compare the two mode theory models. The absolute amplitude of the EMP2D results cannot be used as a check on the other models—only changes in relative amplitude along the propagation path.

For the combinations of h' and β that represent the "typical" day or night D-layer of the ionosphere, all three models are in good agreement (the dark regions of all three panels). Unsurprisingly, the mode theory models are more similar to each other than to the FDTD model. Fig. 6 plots electric field amplitude and phase along the ground for h'=78, $\beta=0.4$, which is representative of the typical ionosphere scenarios. The root mean square difference (RMSD) between LMP and EMP2D for the entire path is 2.29 dB and 11.3° after shifting EMP2D to minimize the Euclidean distance, and the RMSD between LMP and LWPC is 0.27 dB, 1.6°.

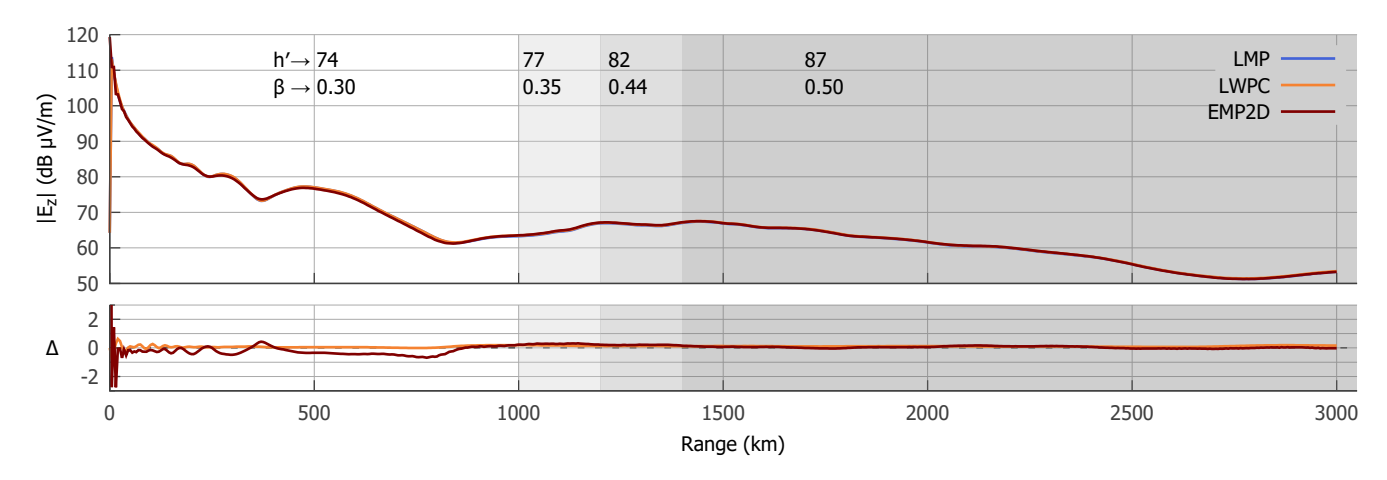


Fig. 8. Electric field amplitude along the ground for a simple day-to-night ionosphere transition over ocean-like ground. The h' and β parameters for each homogeneous ionosphere segment are marked on the figure with the four segments shaded in increasingly darker gray for the transition from day to night.

A notable difference between the models is the poor behavior of LWPC for very low β ionospheres ($\beta < 0.2 \,\mathrm{km}^{-1}$). Such ionospheres may not occur frequently in the real world, but they can occur when using non-linear methods to estimate the ionosphere profile from VLF observations. Some methods represent the estimate as a distribution or are otherwise unbounded [74]. It is therefore important that the propagation model return a reasonable estimate at low β , or at least not throw an error. Fig. 7 plots the electric field amplitude for the $h' = 70, \beta = 0.15$ scenario. In this figure, EMP2D is shifted to minimize its Euclidean distance to LMP alone, but it is clear that the slope of the amplitude line for LMP is a better match to the EMP2D curve than LWPC is. However, LMP still misses the null past 500 km that is present in EMP2D. Expanding the mode search region does not noticeably improve the LMP fit to EMP2D, nor does using a finer initial mesh grid. All of the eigenangles in the search region are already identified using the default mesh. Although it is unclear why the mode theory results are different from the FDTD results, the mode finder itself does not appear to be the reason.

B. Inhomogeneous Ionosphere

To model most realistic ionospheres along a long propagation path, it is necessary to incorporate changes in the ionosphere along the path. LMP and LWPC do this by segmenting the ionosphere into homogeneous segments and using mode conversion to propagate the transmitted wave from one segment into the next. This section demonstrates propagation through a day-to-night transition with two segments along the terminator for a total of four homogeneous ionospheres along the entire propagation path. LMP uses its default parameters with the ionosphere defined as a BasicInput and LWPC used the range-exponential ionosphere specification with FULLMC specified for mode conversion. EMP2D used the same parameters as in Section IV-A.

Fig. 8 plots the vertical electric field amplitude along the ground for the segmented inhomogeneous ionosphere scenario. All three models are in excellent agreement throughout all four homogeneous segments of ionosphere. The root mean square difference between LMP and EMP2D along the entire

path is 2.26 dB and the root mean square difference between LMP and LWPC is 0.13 dB. This is a confirmation that mode conversion is correctly implemented in the Longwave Mode Propagator. Additionally, it demonstrates that ignoring back-propagating reflections from each segment boundary is a valid approximation made by the FULLMC method for a typical inhomogeneous ionosphere. EMP2D naturally includes the effect of such reflections, yet it is in excellent agreement with both models.

C. Magnetic Field Direction

EMP2D is only capable of modeling vertical magnetic fields due to its axisymmetric construction, but Earth's magnetic field direction has a well-known influence on the propagation of longwaves in the EIWG [75], [76]. Both LMP and LWPC are capable of modelling general magnetic field vectors. Nine scenarios were run to compare the influence of magnetic field direction on propagation between these two models. The first scenario used a vertical magnetic field. The next eight scenarios used a dip angle of 60° down from the horizon and varied the azimuth angle in 45° increments. 0° north azimuth is aligned along the propagation path and the azimuth angle increments toward the east. A nighttime ionosphere with h' = 82 and $\beta = 0.6$ was used for each scenario.

Fig. 9 shows the vertical electric field amplitude from LMP for each magnetic field direction. The amplitude differences from the LWPC results are plotted below. There is excellent agreement between the two models. Spikes in the difference plot are caused by small differences in the exact range at which amplitude nulls occur. As expected, there is a significant difference between east-west (pink, relatively higher amplitude) and west-east (green, relatively lower amplitude) paths, while there is no dependence on the north-south direction; the 0° and 180°, 45° and 135°, and 225° and 315° lines are plotted over one another because they are north-south mirrors. The black colored amplitude curve is for the vertical magnetic field vector and is very similar to the 0° and 180° curves.

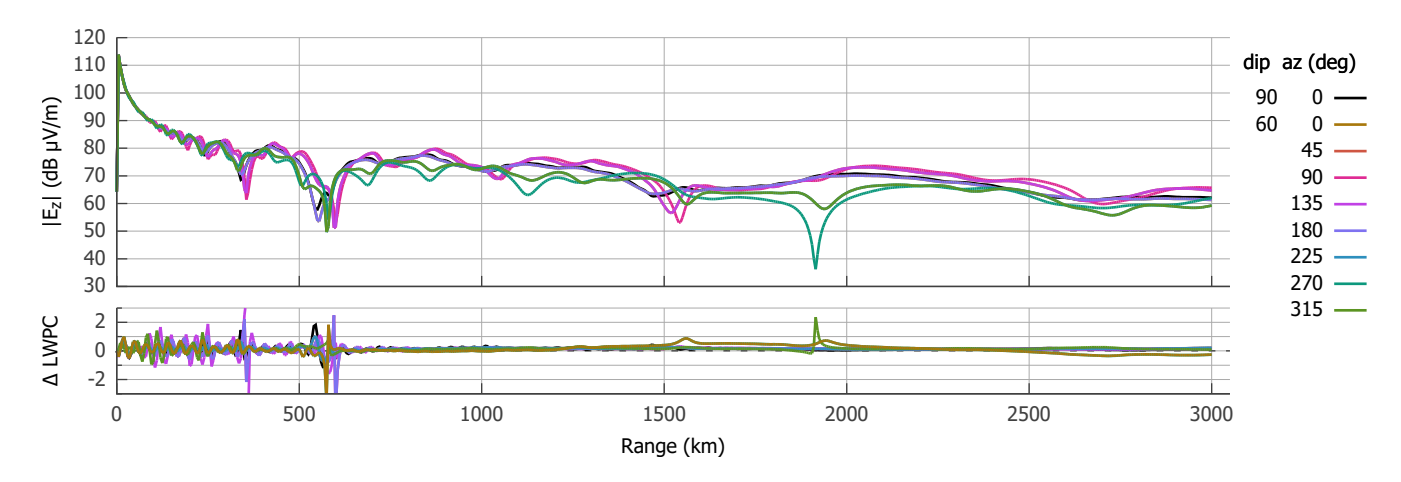


Fig. 9. Electric field amplitude for different magnetic field directions with respect to the propagation path as computed by the Longwave Mode Propagator. The black colored curve is for a vertical magnetic field vector and the other curves all have a dip angle of 60° . The differences between LWPC and LMP are plotted underneath. The ionosphere for each scenario uses a Wait profile with h' = 82 and $\beta = 0.6$, there is an ocean-like ground, and the transmitter is at 24 kHz.

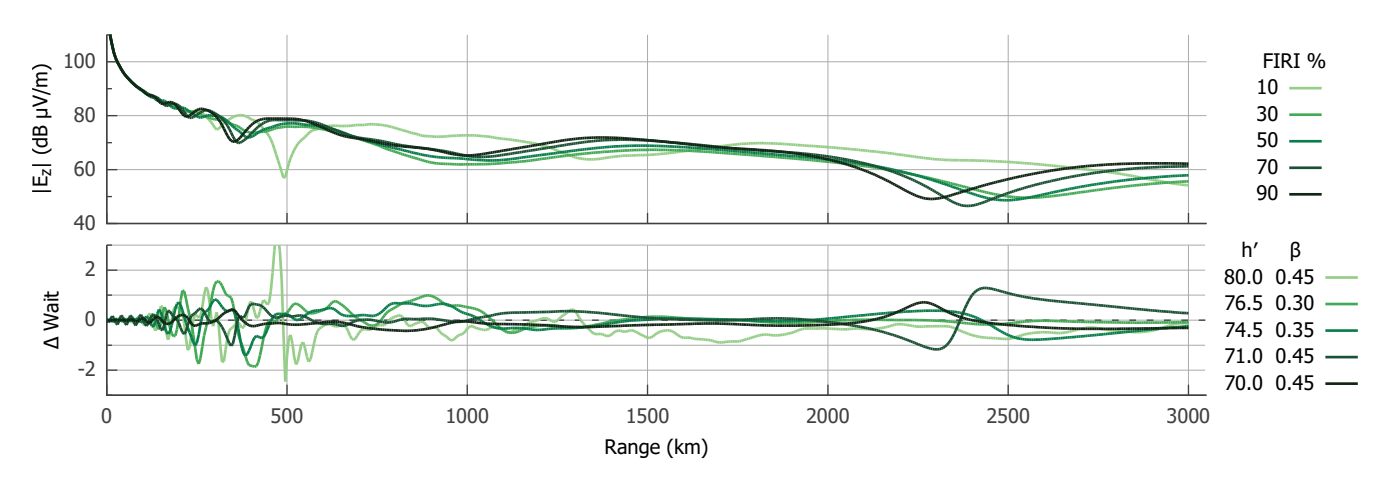


Fig. 10. Top: Electric field amplitude for electron density percentiles of the FIRI profiles. Bottom: The amplitude difference between the FIRI profiles and the corresponding best-fit Wait profiles.

D. Comparing Wait and FIRI Profiles

All of the scenarios shown so far have used the exponential electron density profile attributed to Wait [44]. However, real ionosphere profiles are likely more complicated than this simple two-parameter model suggests [77], [78]. Friedrich et al. [73] presents an update to the semiempirical Faraday-International Reference Ionosphere (FIRI) model for electron density in the lower ionosphere. The FIRI-2018 model blends HF wave propagation and Langmuir probe measurements from sounding rockets with a simple ion-chemical model. Ultimately, it is claimed to be valid for altitudes above 60 km and electron densities above $10^6 \,\mathrm{m}^{-3}$ [73]. Measurements of the signal propagated from VLF transmitters provides a relatively inexpensive and persistent means of probing the lower ionosphere. However, the retrieval of electron density profiles from this technique is underdetermined and it is difficult to accurately fit a profile with more than two parameters. In this section, we compare the fields that result from the Wait and FIRI-2018 electron density profiles. LongwaveModePropagator.jl makes it particularly easy to define arbitrary functional or tabular profiles.

Rather than looking at the explicit influence of latitude, solar activity, or day of year, the FIRI-2018 profiles were separated into day and night by solar zenith angle and averaged over the other parameters. New profiles representing 10, 30, 50, 70, and 90th percentiles of electron density at each altitude were formed for day and night. In this section, we'll be looking at the daytime profiles only. Additionally, an exponential extrapolation was performed from the bottom of the FIRI profiles down to 40 km; some studies have found that VLF propagation is sensitive to the low electron densities at these lower altitudes [78], [79].

Electric field amplitude curves from the five FIRI profiles are shown in Fig. 10. The curves all have broadly similar shapes except for the 10th percentile of electron density. To compare to the Wait profile, LMP was run for a dense grid of parameters with h' from 62 to 90 km in 0.5 km increments and β from 0.2 to $1.6\,\mathrm{km^{-1}}$ in $0.05\,\mathrm{km^{-1}}$ increments. The vertical electric field amplitude was sampled along the entire path from the transmitter in 5 km increments out to $3000\,\mathrm{km}$ for both the FIRI and Wait profiles. The Euclidean distance between these amplitudes for each combination of h' and

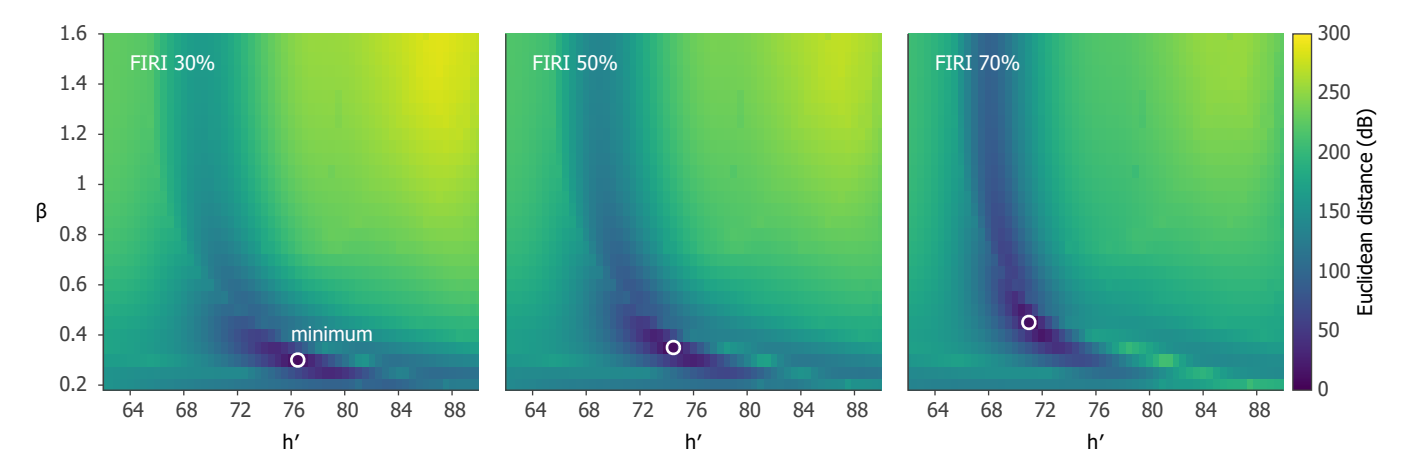


Fig. 11. The Euclidean distance of the amplitude curves between Wait ionosphere profiles and the 30, 50, and 70th percentile FIRI profiles. The best-fit Wait profiles are marked with white circles.

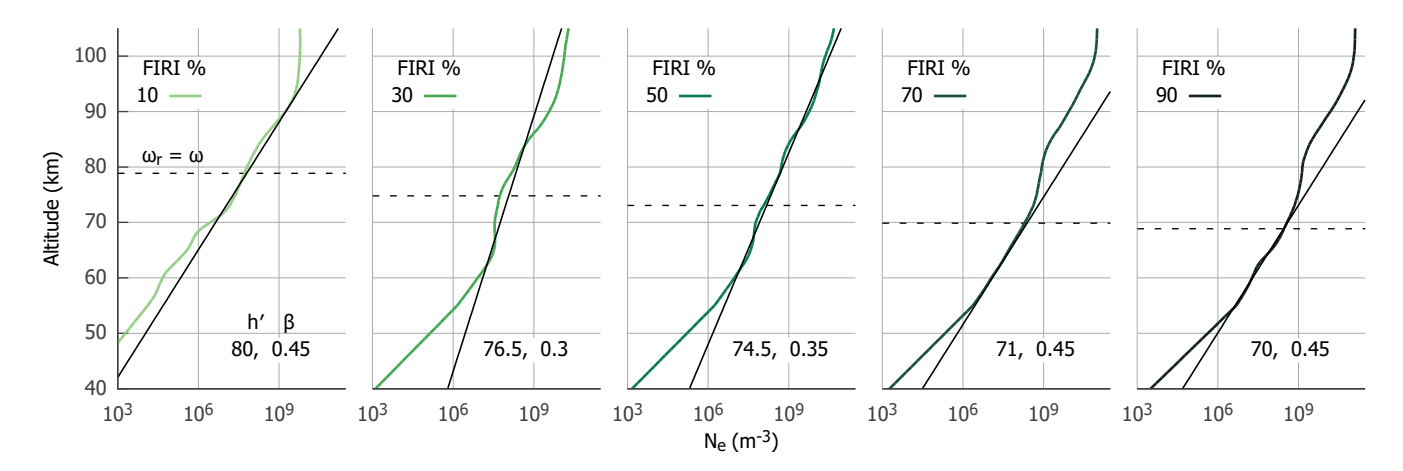


Fig. 12. Percentile electron density profiles of the FIRI model and their corresponding best-fit Wait profiles. The dashed lines indicate the altitudes at which Wait's conductivity parameter ω_r equals the angular wave frequency ω for a 24 kHz wave; this is an approximation of the reflection altitude.

 β are compared to each FIRI profile. An example of the results for the 30, 50, and 70th percentile FIRI profiles are shown in Fig. 11. The minimum identified in each panel is the h' and β ionosphere that minimizes the Euclidean distance between the two amplitude profiles and thus provides a best fit to the FIRI ionosphere. This suggests that perhaps the Wait parameters could be estimated from VLF observations, but used to approximate a more realistic FIRI profile. The amplitude difference between the best-fit Wait profiles and the FIRI profiles are plotted in the bottom of Fig. 10. The difference is within $\pm 1\,\mathrm{dB}$ throughout almost the entire path, with larger errors appearing near nulls in the amplitude pattern.

Fig. 12 shows the FIRI electron density profiles and the corresponding best-fit Wait profiles. The 10th percentile FIRI profile is a good approximation of a Wait profile between 70 km and 90 km altitude. The 30 and 50th percentile FIRI profiles are also similar to their best-fit Wait profiles, except for a deviation below 60 km. At these lower altitudes, an exponential extrapolation is used for the FIRI profiles and there is a much lower electron density than the Wait best-fits. In other words, a much higher electron density was present at low altitudes for the Wait profiles. This was also true to a lesser extent for the 70 and 90th percentile FIRI profiles. However,

in these two profiles, there is also a significant reduction in electron density above 70 km compared to the best-fit Wait profiles. This suggests that VLF is less sensitive to the electron density above these altitudes. Although only an approximation for reflection height, the altitude at which Wait's conductivity parameter is equal to the angular wave frequency is marked with dashed lines in Fig. 12. These heights occur just below the altitudes at which the 70 and 90th percentile FIRI profiles diverge from the Wait profiles. These results provide insight into the altitude range over which the VLF signal amplitude is sensitive to the *D*-layer electron density.

V. Conclusion

We have developed a modern, open source program for the propagation of long radio waves in the Earth-ionosphere waveguide. Compared to LWPC, it uses an entirely different mode finder that is more robust and simplifies the problem solution. In this paper we have discussed the model physics and presented sample scenarios where results from the new Longwave Mode Propagator are compared to the LWPC model and the EMP2D FDTD model. All three are in good agreement for typical VLF-derived electron density profiles. We also show that percentiles of the FIRI-2018 ionosphere model have

uniquely corresponding exponential Wait profiles as determined by VLF amplitude along a homogeneous propagation path. VLF propagation appears to be most sensitive to the electron density profile just below the approximate reflection height where Wait's conductivity parameter ω_r is equal to the angular wave frequency. Further investigation is required to determine how accurately a retrieved Wait profile could be matched to a more realistic profile of the lower ionosphere.

There are opportunities to improve the Longwave Mode Propagator software package. The greatest downside to using the package as opposed to LWPC may be its runtime. However, it might be possible to combine aspects of both mode finding algorithms to more efficiently locate roots and poles. Rather than a brute force search of a dense mesh grid, lines of constant phase could be followed, similar to [38], but then the discretized argument principle could be applied to determine if a root or pole has been located. One would need to be careful not to reduce the robustness of Longwave Mode Propagator's current algorithm, but there is potential to greatly reduce the runtime without sacrificing the simplicity of solving the physical mode equation. Interpolation of the ionosphere reflection coefficient would also reduce the runtime. There are numerous other possible enhancements, including calculating the wave fields higher into the ionosphere, convenience functions for Earth conductivity and magnetic field maps, inhomogeneous ground, and specialized handling of ELF and LF emitters. Anyone is welcome to submit issues or pull requests with enhancements on the package's GitHub page.

ACKNOWLEDGMENT

The authors would like to thank Wei Xu for processing the FIRI-2018 model profiles into day and night percentiles of electron density for use in comparing them to the Wait profile.

REFERENCES

- R. Barr, D. L. Jones, and C. J. Rodger, "ELF and VLF radio waves," Journal of Atmospheric and Solar-Terrestrial Physics, vol. 62, no. 17, pp. 1689–1718, Nov. 2000.
- [2] E. R. Swanson, "ELF-VLF applications in navigation and communications," in *ELF-VLF Radio Wave Propagation*, ser. NATO Advanced Study Institutes Series, J. A. Holtet, Ed. Dordrecht-Holland: D. Reidel Publishing Company, 1974, pp. 371–384.
- [3] P. B. Morris, R. R. Gupta, R. S. Warren, and P. M. Creamer, *Omega Navigation System Course Book*. Reading, MA: The Analytic Sciences Corp., Jul. 1994, vol. 1.
- [4] —, Omega Navigation System Course Book. Reading, MA: The Analytic Sciences Corp., Jul. 1994, vol. 2.
- [5] L. B. Pedersen, L. Persson, M. Bastani, and S. Byström, "Airborne VLF measurements and mapping of ground conductivity in Sweden," *Journal of Applied Geophysics*, vol. 67, no. 3, pp. 250–258, Mar. 2009.
- [6] F. Simões, R. Pfaff, J.-J. Berthelier, and J. Klenzing, "A review of low frequency electromagnetic wave phenomena related to troposphericionospheric coupling mechanisms," *Space Science Reviews*, vol. 168, pp. 551–593, Jun. 2012.
- [7] I. Silber and C. Price, "On the use of VLF narrowband measurements to study the lower ionosphere and the mesosphere-lower thermosphere," *Surveys in Geophysics*, vol. 38, no. 2, pp. 407–441, Mar. 2017.
- [8] J. P. Hauser and F. J. Rhoads, "Coverage predictions for the Navy's fixed VLF transmitters:," Naval Research Laboratory, Washington, D.C., NRL Memorandum Report 2884, Sep. 1974.
- [9] J. A. Ferguson and F. P. Snyder, "Long wave propagation assessment," in Operational Decision Aids for Exploiting or Mitigating Electromagnetic Propagation Effects, vol. 453. San Diego, CA: NATO Advisory Group for Aerospace Research & Development, May 1989, p. 10.

- [10] C. M. Crain, "An overview discussion of propagation effects of nuclear environments on VLF-LF communication systems," The Rand Corporation, Santa Monica, CA, Topical Report DNA 3778T, Aug. 1975.
- [11] J. A. Ferguson, "Ionospheric profiles for predicting nighttime VLF/LF propagation: Determination of an effective (exponential) model for use in design and deployment of resources for communication and navigation," Naval Ocean Systems Center, San Diego, CA, Tech. Rep. NOSC/TR-530, Feb. 1980.
- [12] J. Burke, "DARPA positioning, navigation, and timing (PNT) technology and their impacts on GPS users," GPS Advisory Board, Jun. 2019.
- [13] Department of the Navy, "SBIR N211-052: Navigational positioning source using very low frequency signals."
- [14] M. A. Clilverd, N. R. Thomson, and C. J. Rodger, "Sunrise effects on VLF signals propagating over a long north-south path," *Radio Science*, vol. 34, no. 4, pp. 939–948, 1999.
- [15] Z. Cheng, S. A. Cummer, D. N. Baker, and S. G. Kanekal, "Nighttime D region electron density profiles and variabilities inferred from broadband measurements using VLF radio emissions from lightning," *Journal of Geophysical Research: Space Physics*, vol. 111, no. A5, 2006.
- [16] N. C. Gross, M. B. Cohen, R. K. Said, and M. Gołkowski, "Polarization of narrowband VLF transmitter signals as an ionospheric diagnostic," *Journal of Geophysical Research: Space Physics*, vol. 123, no. 1, pp. 901–917, 2018.
- [17] R. A. Pappert, E. E. Gossard, and I. J. Rothmuller, "A numerical investigation of classical approximations used in VLF propagation," *Radio Science*, vol. 2, no. 4, pp. 387–400, Apr. 1967.
- [18] N. G. Lehtinen, T. F. Bell, and U. S. Inan, "Full-wave method of calculation of electromagnetic fields in stratified media," in 2011 International Conference on Electromagnetics in Advanced Applications, Sep. 2011, pp. 327–330.
- [19] R. A. Marshall, "Effect of self-absorption on attenuation of lightning and transmitter signals in the lower ionosphere," *Journal of Geophysical Research: Space Physics*, vol. 119, no. 5, pp. 4062–4076, 2014.
- [20] M. A. Higginson-Rollins and M. B. Cohen, "Exploiting LF/MF signals of opportunity for lower ionospheric remote sensing," *Geophysical Research Letters*, vol. 44, no. 16, pp. 8665–8671, Aug. 2017.
- [21] N. R. Thomson, M. A. Clilverd, and C. J. Rodger, "Daytime midlatitude D region parameters at solar minimum from short-path VLF phase and amplitude," *Journal of Geophysical Research: Space Physics*, vol. 116, no. A3, 2011.
- [22] N. C. Gross and M. B. Cohen, "VLF remote sensing of the D region ionosphere using neural networks," *Journal of Geophysical Research: Space Physics*, vol. 125, no. 1, 2020.
- [23] M. L. V. Pitteway and J. A. Ratcliffe, "Reflexion levels and coupling regions in a horizontally stratified ionosphere," *Philosophical Transactions of the Royal Society of London. Series A, Mathematical and Physical Sciences*, vol. 252, no. 1004, pp. 53–68, Oct. 1959.
- [24] K. G. Budden, Radio waves in the ionosphere. Cambridge University Press, 1961.
- [25] J. J. Simpson and A. Taflove, "A review of progress in FDTD Maxwell's equations modeling of impulsive subionospheric propagation below 300 kHz," *IEEE Transactions on Antennas and Propagation*, vol. 55, no. 6, pp. 1582–1590, Jun. 2007.
- [26] R. A. Marshall, T. Wallace, and M. Turbe, "Finite-difference modeling of very-low-frequency propagation in the Earth-ionosphere waveguide," *IEEE Transactions on Antennas and Propagation*, vol. 65, no. 12, pp. 7185–7197, Dec. 2017.
- [27] N. G. Lehtinen and U. S. Inan, "Radiation of ELF/VLF waves by harmonically varying currents into a stratified ionosphere with application to radiation by a modulated electrojet," *Journal of Geophysical Research: Space Physics*, vol. 113, no. A6, 2008.
- [28] —, "Full-wave modeling of transionospheric propagation of VLF waves," *Geophysical Research Letters*, vol. 36, no. 3, Feb. 2009.
- [29] R. Courant, H. Lewy, and K. Friedrichs, "Über die partiellen differenzengleichungen der mathematischen physik," *Mathematische Annalen*, vol. 100, pp. 32–74, 1928.
- [30] H. Volland, "Comparison between mode theory and ray theory of VLF propagation," *Journal of Research of the National Bureau of Standards*, Section D: Radio Propagation, vol. 65D, no. 4, pp. 357–361, Jul. 1961.
- [31] A. R. Jacobson, X.-M. Shao, and R. Holzworth, "Full-wave reflection of lightning long-wave radio pulses from the ionospheric D region: Numerical model," *Journal of Geophysical Research: Space Physics*, vol. 114, no. A3, 2009.
- [32] X. Shao and A. R. Jacobson, "Model simulation of very low-frequency and low-frequency lightning signal propagation over intermediate ranges," *IEEE Transactions on Electromagnetic Compatibility*, vol. 51, no. 3, pp. 519–525, Aug. 2009.

- [33] J. A. Ferguson, "Status of the Naval Ocean Systems Center's Long Wave Propagation Capability," in *The Effect of the Ionosphere on Radiowave* Signals and Systems Performance, Washington, D.C., May 1990, pp. 505–514
- [34] ——, "Computer programs for assessment of long-wavelength radio communications, version 2.0: User's guide and source files," Space and Naval Warfare Systems Center, San Diego, CA, Technical Document 3030, May 1998.
- [35] W. M. McRae and N. R. Thomson, "VLF phase and amplitude: Daytime ionospheric parameters," *Journal of Atmospheric and Solar-Terrestrial Physics*, vol. 62, no. 7, pp. 609–618, May 2000.
- [36] C. H. Sheddy, R. Pappert, Y. Gough, and W. Moler, "A Fortran program for mode constants in an Earth-ionosphere waveguide," Naval Electronics Laboratory Center, San Diego, CA, Interim Report 683, May 1968.
- [37] R. A. Pappert, W. F. Moler, and L. R. Shockey, "A Fortran program for waveguide propagation which allows for both vertical and horizontal dipole excitation," Naval Electronics Laboratory Center, San Diego, CA, Tech. Rep. NELC-IR-702, Jun. 1970.
- [38] D. G. Morfitt and C. H. Shellman, "MODESRCH', an improved computer program for obtaining ELF/VLF/LF mode constants in an Earth-ionosphere waveguide," Naval Electronics Laboratory Center, San Diego, CA, Tech. Rep. NELC/IR-77T, Oct. 1976.
- [39] J. A. Ferguson and F. P. Snyder, "Approximate VLF/LF waveguide mode conversion model. computer applications: FASTMC and BUMP," Naval Ocean Systems Center, San Diego, CA, Tech. Rep. NOSC-TD-400, Nov. 1980.
- [40] —, "The segmented waveguide program for long wavelength propagation calculations," Naval Ocean Systems Center, San Diego, CA, Tech. Rep. NOSC/TD-1071, Apr. 1987.
- [41] R. R. Schaller, "Moore's law: Past, present and future," *IEEE Spectrum*, vol. 34, no. 6, pp. 52–59, 1997.
- [42] C. H. Shellman, "A new version of MODESRCH using interpolated values of the magnetoionic reflection coefficients," Naval Ocean Systems Center, San Diego, CA, Tech. Rep. NOSC/TR-1143, Aug. 1986.
- [43] R. A. Pappert, "LF daytime earth ionosphere waveguide calculations," Naval Ocean Systems Center, San Diego, CA, Tech. Rep. NOSC/TR-647, Jan. 1981.
- [44] J. R. Wait and K. P. Spies, "Characteristics of the Earth-ionosphere waveguide for VLF radio waves," U.S. National Bureau of Standards, Boulder, CO, Technical Note 300, Dec. 1964.
- [45] M. Hutchins, "LWPC," Oct. 2016. [Online]. Available: https://github.com/mlhutchins/LWPC
- [46] P. Kowalczyk, "Global complex roots and poles finding algorithm based on phase analysis for propagation and radiation problems," *IEEE Transactions on Antennas and Propagation*, vol. 66, no. 12, pp. 7198–7205, Dec. 2018.
- [47] G. N. Watson, "The transmission of electric waves round the Earth," Proceedings of the Royal Society of London. Series A, Containing Papers of a Mathematical and Physical Character, vol. 95, no. 673, pp. 546– 563. Jul. 1919.
- [48] J. E. Best, J. A. Ratcliffe, and M. V. Wilkes, "Experimental investigations of very long waves reflected from the ionosphere," *Proceedings of the Royal Society of London. Series A - Mathematical and Physical Sciences*, vol. 156, no. 889, pp. 614–633, Sep. 1936.
- [49] K. G. Budden, "The numerical solution of differential equations governing reflexion of long radio waves from the ionosphere," *Proc. R. Soc. Lond. A*, vol. 227, no. 1171, pp. 516–537, Feb. 1955.
- [50] ——, "The influence of the earth's magnetic field on radio propagation by wave-guide modes," *Proceedings of the Royal Society of London. Series A. Mathematical and Physical Sciences*, vol. 265, no. 1323, pp. 538–553, Feb. 1962.
- [51] N. R. Thomson, "Experimental daytime VLF ionospheric parameters," *Journal of Atmospheric and Terrestrial Physics*, vol. 55, no. 2, pp. 173– 184, Feb. 1993.
- [52] R. A. Pappert and R. R. Smith, "Orthogonality of VLF height gains in the earth ionosphere waveguide," *Radio Science*, vol. 7, no. 2, pp. 275–278, 1972.
- [53] K. G. Budden, The wave-guide mode theory of wave propagation. Prentice-Hall, 1961.
- [54] B. K. Banerjea, "On the propagation of electromagnetic waves through the atmosphere," *Proceedings of the Royal Society of London. Series A. Mathematical and Physical Sciences*, vol. 190, no. 1020, pp. 67–81, Jun. 1947.
- [55] P. C. Clemmow and J. Heading, "Coupled forms of the differential equations governing radio propagation in the ionosphere," *Mathematical*

- Proceedings of the Cambridge Philosophical Society, vol. 50, no. 2, pp. 319–333, Apr. 1954.
- [56] K. G. Budden, The propagation of radio waves: The theory of radio waves of low power in the ionosphere and magnetosphere. Cambridge University Press, Aug. 1988.
- [57] J. A. Ratcliffe, The magneto-ionic theory & its applications to the ionosphere. Cambridge University Press, 1959.
- [58] H. G. Booker and W. Walkinshaw, "The mode theory of tropospheric refraction and its relation to wave-guides and diffraction," *Meteorological factors in radio-wave propagation*, pp. 80–127, Apr. 1946.
- [59] R. A. Pappert, "A numerical study of VLF mode structure and polarization below an anisotropic ionosphere," *Radio Science*, vol. 3, no. 3, pp. 219–233, Mar. 1968.
- [60] C. H. Sheddy, "A general analytic solution for reflection from a sharply bounded anisotropic ionosphere," *Radio Science*, vol. 3, no. 8, pp. 792– 795, Aug. 1968.
- [61] H. G. Booker, "Propagation of wave-packets incident obliquely upon a stratified doubly refracting ionosphere," *Philosophical Transactions* of the Royal Society of London. Series A, Mathematical and Physical Sciences, vol. 237, no. 781, pp. 411–451, Sep. 1938.
- [62] I. W. Yabroff, "Reflection at a sharply-bounded ionosphere," Proceedings of the IRE, vol. 45, no. 6, pp. 750–753, Jun. 1957.
- [63] J. Skowron and A. Gould, "General complex polynomial root solver and its further optimization for binary microlenses," 2012. [Online]. Available: https://arxiv.org/abs/1203.1034
- [64] J. Lekner, Theory of reflection of electromagnetic and particle waves. Dordrecht: Springer Netherlands, 1987.
- [65] The staff of the computation library, Tables of the modified Hankel function of order one-third and of their derivatives, ser. The Annals of the Computation Laboratory of Harvard University. Cambridge, MA: Harvard University Press, 1945, vol. 2.
- [66] R. A. Pappert and L. R. Shockey, "WKB mode summing program for VLF/ELF antennas of arbitrary length, shape and elevation," Naval Electronics Laboratory Center, San Diego, CA, Interim Report NELC-IR-713, M402, Jun. 1971.
- [67] R. A. Pappert, L. R. Hitney, and J. A. Ferguson, "ELF/VLF long path pulse program for antennas of arbitrary elevation and orientation," Naval Ocean Systems Center, San Diego, CA, Tech. Rep. NOSC/TR-891, Aug. 1983.
- [68] R. A. Pappert and L. R. Shockey, "Simplified VLF/LF mode conversion program with allowance for elevated, arbitrarily oriented electric dipole antennas," Naval Electronics Laboratory Center, San Diego, CA, Interim Report 771, Oct. 1976.
- [69] —, "Mode conversion program for an inhomogeneous anisotropic ionosphere," Naval Electronics Laboratory Center, San Diego, CA, Tech. Rep. NELC-IR-722, May 1972.
- [70] M. L. V. Pitteway, "The numerical calculation of wave-fields, reflexion coefficients and polarizations for long radio waves in the lower ionosphere. I." *Phil. Trans. R. Soc. Lond. A*, vol. 257, no. 1079, pp. 219–241, Mar. 1965.
- [71] C. Rackauckas and Q. Nie, "Differential equations.jl a performant and feature-rich ecosystem for solving differential equations in Julia," *The Journal of Open Research Software*, vol. 5, no. 1, 2017.
- [72] F. Gasdia, "fgasdia/rootsandpoles.jl: v1.4.0," 2020. [Online]. Available: https://github.com/fgasdia/RootsAndPoles.jl
- [73] M. Friedrich, C. Pock, and K. Torkar, "FIRI-2018, an updated empirical model of the lower ionosphere," *Journal of Geophysical Research: Space Physics*, vol. 123, no. 8, pp. 6737–6751, 2018.
- [74] F. Gasdia and R. A. Marshall, "Assimilating VLF transmitter observations with an LETKF for spatial estimates of the D-region ionosphere," *IEEE Transactions on Geoscience and Remote Sensing*, pp. 1–18, 2019.
- [75] D. D. Crombie, "Differences between the east-west and west-east propagation of VLF signals over long distances," *Journal of Atmospheric* and *Terrestrial Physics*, vol. 12, no. 2, pp. 110–117, Jan. 1958.
- [76] A. E. Chand and S. Kumar, "VLF modal interference distance and nighttime D region VLF reflection height for west-east and east-west propagation paths to Fiji," *Radio Science*, vol. 52, no. 8, pp. 1004–1015, Aug. 2017.
- [77] G. Bainbridge and U. S. Inan, "Ionospheric D region electron density profiles derived from the measured interference pattern of VLF waveguide modes," *Radio Science*, vol. 38, no. 4, Aug. 2003.
- [78] D. E. Siskind, K. A. Zawdie, F. Sassi, D. P. Drob, and M. Friedrich, "An intercomparison of VLF and sounding rocket techniques for measuring the daytime D region ionosphere: Theoretical implications," *Journal of Geophysical Research: Space Physics*, vol. 123, no. 10, pp. 8688–8697, 2018.

[79] W. Xu, R. A. Marshall, A. Kero, E. Turunen, D. Drob, J. Sojka, and D. Rice, "VLF measurements and modeling of the D-region response to the 2017 total solar eclipse," *IEEE Transactions on Geoscience and Remote Sensing*, vol. 57, no. 10, pp. 7613–7622, Oct. 2019.



Forrest Gasdia received the B.S. and M.S. degrees in engineering physics from Embry-Riddle Aeronautical University, Daytona Beach, FL, in 2014 and 2016, and the M.S. degree in aerospace engineering sciences at University of Colorado Boulder, Boulder, CO, in 2020. He is currently a Ph.D. candidate in aerospace engineering sciences at University of Colorado Boulder.



Robert A. Marshall (SM'07–M'15) received the B.S. degree in electrical engineering from the University of Southern California, Los Angeles, in 2002, and the M.S. and Ph.D. degrees in electrical engineering from Stanford University, Stanford, CA, in 2004 and 2009. He is currently an Assistant Professor in the Ann and H.J. Smead Department of Aerospace Engineering Sciences at the University of Colorado Boulder, in Boulder, CO.

He has previously held research positions in the Center for Space Physics at Boston University and

the department of Aeronautics and Astronautics at Stanford University. He is an author of the book "Numerical Electromagnetics: The FDTD Method" (Cambridge University Press, 2011) with U.S. Inan. His current research activities include the study of lightning-ionosphere interactions; radiation belt precipitation and atmospheric effects; numerical modeling and applications in space physics; and small satellite instrument development.

Dr. Marshall received First Place in the 2007 International Radio Science Union (URSI) Student Paper Competition, and was a recipient of the URSI Young Scientist Award in 2011.